Nuclear Science and Techniques (2026) 37:105
https://doi.org/10.1007/s41365-026-01937-y

Investigation of the isotopic dependence in the synthesis of superheavy nuclei with plutonium and curium targets

Ming-Hao Zhang[1,2] · Mei-Chen Wang[1,2] · Ying Zou[1,2] · Gen Zhang[3] · Qing-Lin Niu[1,2] · Feng-Shou Zhang[1,2,4]

Received: 11 December 2024 / Revised: 16 August 2025 / Accepted: 3 September 2025 / Published online: 26 March 2026

Abstract

In the synthesis of new superheavy nuclei, the various long half-lives of Pu and Cm isotopes render them promising target materials for fusion reactions. Investigating the isotopic dependence of actinide targets is important for selecting optimal reaction systems. Based on the dinuclear system model, the impact of the target isotope is investigated for the reactions ^{48}Ca + ^{239,240,242,244}Pu. The reaction systems with the $^{242-248}$Cm targets and the ^{45}Sc, ^{50}Ti, ^{51}V, ^{54}Cr, ^{55}Mn projectiles are investigated for the synthesis of new isotopes $^{284-290}$Ts, $^{289-293,295}$Og, $^{290-296}$119, $^{293-299}$120, $^{294-300}$121. The isotopic dependence of the Cm targets revealed an ascending trend of the maximal ER cross section coupled with an odd–even effect as the neutron number of the target increased, and the ^{247}Cm target emerged as promising for future experiments. The optimal reactions for producing new superheavy elements with $Z = 119$–121 are predicted to be the reactions ^{51}V + ^{245}Cm, ^{54}Cr + ^{247}Cm, and ^{55}Mn + ^{247}Cm with maximal ER cross sections of 144 fb, 0.877 fb, and 0.052 fb, respectively.

Keywords Superheavy nuclei · Dinuclear system model · Fusion reaction · Isotopic dependence

1 Introduction

The synthesis and investigation of unknown superheavy elements (SHEs) can reveal the shell structure and decay properties near the predicted "island of stability" [1–5]. Over recent decades, remarkable advancements have been achieved in the synthesis of new SHEs with $Z = 114$–118 through fusion reactions with the ^{48}Ca projectile and the actinide targets [6–11]. To date, modern accelerators coupled with sensitive detection techniques have made notable progress in the synthesis of new superheavy nuclei [12–20]. Despite these advances, a significant gap remains in the superheavy nuclei region, necessitating continued experimental and theoretical investigations.

For synthesizing new superheavy nuclei, the ^{48}Ca-induced fusion reactions encounter constraints due to the limited amount of experimental feasible Bk and Cf targets. Consequently, employing combinations of Cm targets and heavier stable projectiles can be an alternative for future experiments. The mixed-Cm target material was produced by irradiating the plutonium target at the Savannah River Site, with subsequent recovery at the Oak Ridge National Laboratory [21]. With long half-lives ranging from decades to millions of years, many Pu and Cm isotopes have been extensively applied as target materials in fusion reactions aimed at synthesizing new isotopes [14, 22–37]. In 2022, the reaction ^{51}V + ^{248}Cm was attempted to synthesize a new element with $Z = 119$, and the optimal reaction energy for this reaction was estimated [38]. These experiments revealed the critical influence of the target neutron

This work was supported by the National Key R&D Program of China (No. 2023YFA1606401), the National Natural Science Foundation of China (Nos. 12135004, 11635003, and 11961141004), and the Guangxi Natural Science Foundation (No. 2022GXNSFBA035549).

✉ Feng-Shou Zhang
fszhang@bnu.edu.cn

1 The Key Laboratory of Beam Technology of Ministry of Education, School of Physics and Astronomy, Beijing Normal University, Beijing 100875, China

2 Institute of Radiation Technology, Beijing Academy of Science and Technology, Beijing 100875, China

3 School of Physical Science and Technology, Guangxi University, Nanning 530004, China

4 Center of Theoretical Nuclear Physics, National Laboratory of Heavy Ion Accelerator of Lanzhou, Lanzhou 730000, China

excess on the maximal ER cross sections, indicating the necessity for further research into the isotopic dependence of target materials.

Based on the experimental results, a variety of theoretical models, including both the macroscopic [39–44] and the microscopic approaches [45–51], have been developed. Among these, the dinuclear system (DNS) model has been proven to be reliable in investigating the fusion-evaporation reactions [52–62]. Within the framework of the DNS model, the fusion-evaporation process is divided into three stages: initial formation of the DNS upon overcoming the Coulomb barrier by the colliding nuclei; subsequent production of a compound nucleus through nucleon transfer from the lighter projectile to the heavier target; and finally, the synthesis of a superheavy nucleus via the evaporation of neutrons by the excited compound nucleus to reach the ground state.

Experiments have revealed that the evaporation residual (ER) cross sections of fusion reactions exhibit remarkable sensitivity to the selection of the target material [14, 63]. The isotopic dependence of the target not only affects the ER cross sections for synthesizing new superheavy nuclei but also influences their decay properties and the feasibility of observation for a sufficient duration to study their chemical and physical properties. Therefore, to search for the optimal projectile–target combinations, it is necessary to investigate the isotopic dependence of the target materials. Based on the DNS model, this study discusses the isotopic dependence of the targets and investigates the potential for extending the superheavy nuclei region with Cm targets.

The remainder of this article is organized as follows: in Sect. 2, we describe the theoretical framework of the DNS model. In Sect. 3, the reliability of the DNS model is examined based on the ample experimental results of the fusion reactions ^{48}Ca + ^{239,240,242,244}Pu, with an investigation into the influence of the target isotope on the capture, fusion, and survival stages. Additionally, the experimental results of the reactions ^{48}Ca + ^{245,248}Cm are compared with the theoretical calculations. The combinations of the $^{242-248}$Cm target and the ^{45}Sc, ^{50}Ti, ^{51}V, ^{54}Cr, and ^{55}Mn projectiles were investigated for extending the superheavy nuclei region with Z = 117–121, presenting the maximal ER cross sections and corresponding incident energies. The isotopic dependence of the Cm targets was discussed in detail for the capture, fusion, and survival stages. In Sect. 4, a summary of this study is provided.

2 Theoretical descriptions

Within the framework of the DNS model, the ER cross section as a function of the center-of-mass energy $E_{\mathrm{c.m.}}$ is calculated by summing the contributing partial waves J [64]:

$$\sigma_{\mathrm{ER}}(E_{\mathrm{c.m.}}) = \frac{\pi\hbar^2}{2\mu E_{\mathrm{c.m.}}}\sum_J (2J+1)T(E_{\mathrm{c.m.}},J) \times P_{\mathrm{CN}}(E_{\mathrm{c.m.}},J)W_{\mathrm{sur}}(E_{\mathrm{c.m.}},J). \tag{1}$$

In this formula, $T\left(E_{\mathrm{c.m.}},J\right)$ is the transmission probability for the formation of the dinuclear system. $P_{\mathrm{CN}}\left(E_{\mathrm{c.m.}},J\right)$ denotes the probability of complete fusion into a compound nucleus [65]. $W_{\mathrm{sur}}\left(E_{\mathrm{c.m.}},J\right)$ represents the probability that the excited compound nucleus survives fission [66]. The interaction potential of the colliding nuclei is given as follows:

$$V(R,\beta_1,\beta_2,\theta_1,\theta_2) = \frac{1}{2}C_1(\beta_1-\beta_1^0)^2 + \frac{1}{2}C_2(\beta_2-\beta_2^0)^2 + V_{\mathrm{C}}(R,\beta_1,\beta_2,\theta_1,\theta_2) + V_{\mathrm{N}}(R,\beta_1,\beta_2,\theta_1,\theta_2). \tag{2}$$

Here, $\beta_{1,2}^0$ indicates the corresponding static deformations, which are usually considered the quadrupole deformation parameters of the nucleus [1]. $C_{1,2}$ denotes the stiffness of the nuclear surface predicted by the liquid-drop model [67, 68]. Assuming that the deformation energy is proportional to the mass number $\frac{C_1\beta_1^2}{C_2\beta_2^2} = \frac{A_1}{A_2}$, the dynamical deformations of the two nuclei can be expressed in terms of the total dynamical deformation parameter $\beta = \beta_1 + \beta_2$. $\beta_0 = \beta - \beta_1^0 - \beta_2^0$ represents the additional deformation beyond the static values, which is distributed between the projectile and target according to the above relation derived from the energy minimization condition:

$$\beta_1 = \frac{B_0}{1+B_0}\beta_0 + \beta_1^0, \tag{3}$$

$$\beta_2 = \frac{1}{1+B_0}\beta_0 + \beta_2^0, \tag{4}$$

with $B_0 = \beta_1/\beta_2 = \sqrt{A_1C_2/A_2C_1}$ is a weighting coefficient.

The Coulomb potential V_{C} is calculated using the Wong formula [69]:

$$V_{\mathrm{C}}(R,\beta_1,\beta_2,\theta_1,\theta_2) = \frac{Z_1Z_2e^2}{R} + \sqrt{\frac{9}{20\pi}}\frac{Z_1Z_2e^2}{R^3} \times \sum_{i=1,2} R_i^2\beta_i P_2(\cos\theta_i) + \frac{3}{7\pi}\frac{Z_1Z_2e^2}{R^3} \times \sum_{i=1,2} R_i^2[\beta_i P_2(\cos\theta_i)]^2. \tag{5}$$

The nuclear potential V_{N} is described by a sudden-approximation double-folding potential [70]:

$$V_N(\mathbf{R}) = C_0\left\{\frac{F_{in}-F_{ex}}{\rho_0}\left[\int \rho_1^2(\mathbf{r})\rho_2(\mathbf{r}-\mathbf{R})d\mathbf{r} + \int \rho_1(\mathbf{r})\rho_2^2(\mathbf{r}-\mathbf{R})d\mathbf{r}\right.\right. \left.\left. + F_{ex}\int \rho_1(\mathbf{r})\rho_2(\mathbf{r}-\mathbf{R})d\mathbf{r}\right]\right\}, \tag{6}$$

with

$$F_{in,ex} = f_{in,ex} + f'_{in,ex}\frac{N_1-Z_1}{A_1}\frac{N_2-Z_2}{A_2}. \tag{7}$$

Here $C_0 = 300$ MeV·fm^3, $f_{in} = 0.09$, $f_{ex} = -2.59$, $f'_{in} = 0.42$ and $f'_{ex} = 0.54$ [70]. The nuclear densities are expressed as two-parameter Woods–Saxon forms with a deformed radius:

$$\rho_1(\mathbf{r}) = \frac{\rho_0}{1+\exp\left((\mathbf{r}-\mathfrak{R}_1(\theta_1))/a_1\right)}, \tag{8}$$

$$\rho_2(\mathbf{r}) = \frac{\rho_0}{1+\exp\left((|\mathbf{r}-\mathbf{R}|-\mathfrak{R}_2(\theta_2))/a_2\right)}, \tag{9}$$

with

$$\mathfrak{R}_i(\theta_i) = R_i\left(1+\beta_i Y_2^0(\theta_i)\right). \tag{10}$$

Here, ρ_0=0.17 fm^{-3} and $a_{1,2} = 0.55$ fm. R_i denotes the spherical radii of the nuclei, and $Y_2^0(\theta)$ is the spherical harmonic.

The transmission probability, which represents the capacity of colliding nuclei to surpass the Coulomb barrier, is determined as:

$$T\left(E_{c.m.},J\right) = \int f(B)T\left(E_{c.m.},B,J\right)\mathrm{d}B. \tag{11}$$

$T(E_{c.m.},B,J)$ is given by the Ahmed formula [71–73]. The barrier distribution function *f(B)* is described by an asymmetric Gaussian form [73]:

$$f(B) = \begin{cases} \frac{1}{N}\exp\left[-\left(\frac{B-B_m}{\Delta_1}\right)^2\right], & B < B_m, \\ \frac{1}{N}\exp\left[-\left(\frac{B-B_m}{\Delta_2}\right)^2\right], & B > B_m. \end{cases} \tag{12}$$

Here, B represents the position of the Coulomb barrier. $B_m = aV_B^{Sp} + (1-a)V_B^S$ is given by a weighted combination of the two barrier values. V_B^{Sp} refers to the Coulomb barrier of the spherical nuclei, whereas V_B^S denotes that at the saddle-point. The width parameters Δ_1 and Δ_2 are defined as $\Delta_1 = \frac{b}{2}(C_1(\beta_1^S)^2 + C_2(\beta_2^S)^2)$ and $\Delta_2 = \frac{c}{2}(C_1(\beta_1^S)^2 + C_2(\beta_2^S)^2)$, respectively. The deformation parameters $\beta_{1,2}^S$ correspond to the projectile and target nuclei in the saddle-point configuration. For deformed nuclear systems, the empirical parameters are set as $a = 0.37$, $b = 0.12$, and $c = 1.12$ [74].

The capture cross section σ_{cap} is expressed as follows [75]:

$$\sigma_{cap}\left(E_{c.m.}\right) = \frac{\pi\hbar^2}{2\mu E_{c.m.}}\sum_J (2J+1)T\left(E_{c.m.},J\right). \tag{13}$$

In the DNS model, it is assumed that the two touching nuclei maintain their individual identities, along with their ground-state characteristics and deformations [76]. The nucleon transfer process occurs along the mass asymmetry degree $\eta = (A_1 - A_2)/(A_1 + A_2)$. The nucleon transfer process, involving the dissipation of kinetic energy and angular momentum, occurs at the valley of the potential energy surface, defined as the driving potential [77]. To form a compound nucleus, the dinuclear system must possess sufficient energy to overcome the inner fusion barrier B_{fus}, which is the energy difference between the incident point and the point of the maximal driving potential (B.G. point). Therefore, with the interaction time $\tau_{int}(J)$ given by the deflection function method [78], the fusion probability is obtained by summing the distribution probabilities of the fragments that successfully overcome the inner fusion barrier:

$$P_{CN}(E_{c.m.},J) = \sum_{Z_1=1}^{Z_{B.G.}}\sum_{N_1=1}^{N_{B.G.}} P(Z_1,N_1,E_1,\tau_{int}(J)). \tag{14}$$

Here, the distribution probability $P\left(Z_1,N_1,E_1,t\right)$ is determined by resolving a set of two-dimensional master equations [73]:

$$\begin{aligned} \frac{\mathrm{d}P(Z_1,N_1,E_1,t)}{\mathrm{d}t} &= \sum_{Z'_1} W_{Z_1,N_1;Z'_1,N_1}(t) \\ &\times [d_{Z_1,N_1}P(Z'_1,N_1,E_1,t) - d_{Z'_1,N_1}P(Z_1,N_1,E_1,t)] \\ &+ \sum_{N'_1} W_{Z_1,N_1;Z_1,N'_1}(t) \\ &\times [d_{Z_1,N_1}P(Z_1,N'_1,E_1,t) - d_{Z_1,N'_1}P(Z_1,N_1,E_1,t)] \\ &- [\Lambda_{qf}(\Theta(t)) + \Lambda_{fis}(\Theta(t))]P(Z_1,N_1,E_1,t). \end{aligned} \tag{15}$$

$W_{Z_1,N_1;Z'_1,N_1}$ denotes the mean transition probability from (Z_1,N_1) to (Z'_1,N_1) [79], d_{Z_1,N_1} is the microscopic dimension associated with (Z_1,N_1). Λ_{qf} and Λ_{fis} represents the quasi-fission and fission probabilities obtained using the one-dimensional Kramers formula [80].

For the evaporation of x neutrons, the survival probability is given by the statistical model:

$$W_{\text{sur}}(E^*_{\text{CN}}, x, J) = P(E^*_{\text{CN}}, x, J) \prod_{i=1}^{x} \left[\frac{\Gamma_n(E^*_i, J)}{\Gamma_n(E^*_i, J) + \Gamma_f(E^*_i, J)} \right]. \quad (16)$$

$P(E^*_{\text{CN}}, x, J)$ is the realization probability of emitting x neutrons at excitation energy E^*_{CN} [81]. The realization probability for emitting one neutron is expressed as:

$$P(E^*_{\text{CN}}, 1, J) = \exp\left[-\frac{(E^*_{\text{CN}} - B_n - 2T)^2}{2\sigma^2} \right]. \quad (17)$$

Here, $\sigma = 2.5$ MeV is the half-height width of the excitation function. For multiple neutron emissions, the realization probability can be expressed using the Jackson formula as follows:

$$P(E^*_{\text{CN}}, x, J) = I(\Delta_x, 2x-3) - I(\Delta_{x+1}, 2x-1), \quad (18)$$

where I and Δ are given by

$$I(z, m) = \frac{1}{m!} \int_0^z u^m e^{-u} \text{d}u, \quad (19)$$

$$\Delta_x = \frac{E^*_{\text{CN}} - \sum_{i=1}^{x} B^n_i}{T_i}. \quad (20)$$

Here, B^n_i is the separation energy of the i-th neutron. E^*_i denotes the excitation energy before evaporating the i-th neutron. The partial decay widths for neutron evaporation Γ_n and fission decay Γ_f were determined using the Weisskopf–Ewing theory [82] and the Bohr–Wheeler transition-state method [83], respectively. The level density parameter a can be taken as $a = A/12$ MeV, and $a_f/a = 1.1$. In the calculation of Γ_f, the fission barrier of the rotating nucleus is expressed as:

$$\begin{aligned} B_f(E^*, J) =& B^{\text{LD}}_f (1 - x_{\text{LD}} T^2) \\ &+ B^{\text{M}}_f (E^* = 0, J) \exp\left(-\frac{E^*}{E_D} \right) \\ &- \left(\frac{\hbar^2}{2J_{\text{g.s.}}} - \frac{\hbar^2}{2J_{\text{s.d.}}} \right) J(J+1). \end{aligned} \quad (21)$$

Here, B^{LD}_f denotes the macroscopic part determined by the liquid-drop model. B^{M}_f is the microscopic shell correction [1]. x_{LD} and E_D represent the temperature-dependent parameter and shell damping energy, respectively, as defined in Ref. [84]. The moments of inertia of the compound nucleus in the ground state and at the saddle-point are given by $J_{\text{g.s.;s.d.}} = k\frac{2}{5}mr^2\left(1 + \beta_2^{\text{g.s.;s.d.}}/3\right)$, respectively [85, 86], where $k = 0.4$ is the correction factor for the rigid-body approximation. The quadrupole deformation at the saddle-point is taken as $\beta_2^{\text{s.d.}} = \beta_2^{\text{g.s.}} + 0.2$, with $\beta_2^{\text{g.s.}}$ denoting the quadrupole deformation parameter at the ground state [1]. In this work, we analyze uncertainties arise from the parameterized E_D [73, 87, 88].

3 Results and discussion

3.1 The isotopic dependence of the reactions with ^{239,240,242,244}Pu targets

Given the large amount of available experimental data, Pu-based hot fusion reactions are crucial for assessing theoretical models. Typically, a higher neutron excess in the target leads to an enhanced maximal ER cross section. Figure 1 presents both experimental and theoretical maximal ER cross sections of the 3n- and 4n-emission channels for the reactions ^{48}Ca + ^{239,240,242,244}Pu. An ascending trend was observed in both the experimental and theoretical maximal ER cross sections with an increase in the neutron number in the target. Notably, the maximal ER cross sections of the 4n-emission channel increase more rapidly than those of the 3n-emission channel as the neutron number of the target increases. To understand the isotopic dependence of the target, thorough investigations of the capture, fusion, and survival stages are required.

Figure 2a presents the capture cross sections of the reactions ^{48}Ca + ^{239,240,242,244}Pu at $E^*_{\text{CN}} = 35$, 40 and 45 MeV. This reveals that the capture cross sections increase with increasing E^*_{CN}, owing to the enhanced probability at higher E^*_{CN} for the colliding nuclei to overcome the Coulomb barrier. A slight declining trend in the capture cross sections was observed as the neutron number of the target increased. This can be attributed to the effect of the Coulomb barriers. Figure 2b illustrates the excitation energies associated with the Coulomb barriers $V_B + Q$ for these reactions. It is evident that the $V_B + Q$ values exhibit an upward trend as the neutron

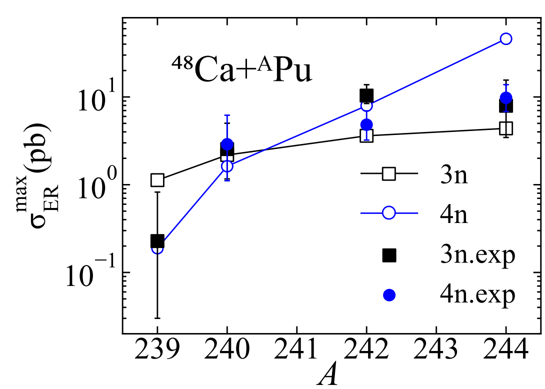

Fig. 1 (Color online) The experimental [22–27, 34, 35] and calculated maximal ER cross sections in the 3n- and 4n-emission channel of the reactions ^{48}Ca + ^{239,240,242,244}Pu→ $^{287,288,290,292-xn}$Fl + xn

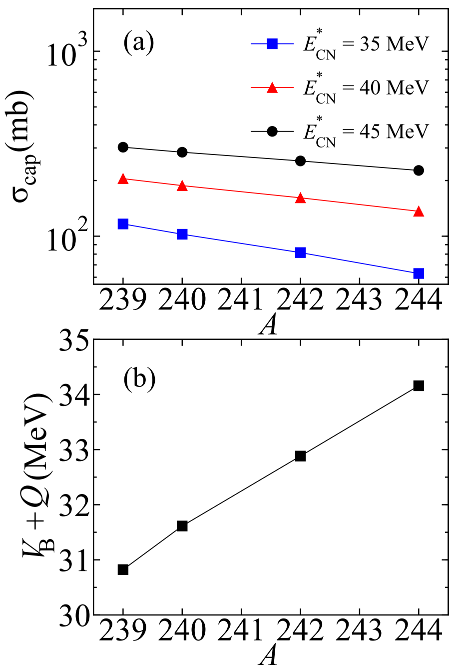

Fig. 2 (Color online) **a** The calculated capture cross sections for the reactions ^{48}Ca + ^{239,240,242,244}Pu→ $^{287,288,290,292-xn}$Fl+xn with E^*_{CN} = 35, 40 and 45 MeV. **b** The excitation energies of the corresponding Coulomb barriers of the reactions ^{48}Ca + ^{239,240,242,244}Pu→ $^{287,288,290,292-xn}$Fl + xn

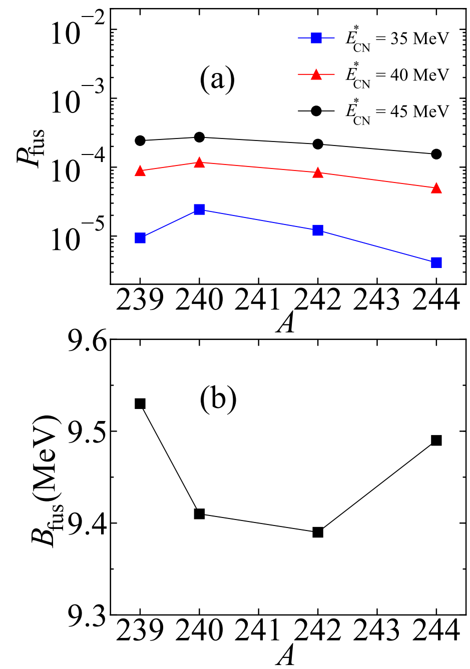

Fig. 3 (Color online) **a** The calculated fusion probabilities for the reactions ^{48}Ca + ^{239,240,242,244}Pu→ $^{287,288,290,292-xn}$Fl + xn with E^*_{CN} = 35, 40 and 45 MeV. **b** The B_{fus} values of the reactions ^{48}Ca + ^{239,240,242,244}Pu→ $^{287,288,290,292-xn}$Fl + xn

number of the target increases, resulting in a decrease in the capture cross section.

For the fusion stage, Fig. 3a illustrates the fusion probabilities for the reactions ^{48}Ca + ^{239,240,242,244}Pu at $E^*_{CN} = 35$, 40 and 45 MeV. The fusion probabilities exhibited a slight decreasing trend with increasing neutron number of the Pu target. Moreover, as the E^*_{CN} increases, the fusion probabilities are enhanced, and the isotopic effect on the fusion probabilities gradually diminishes. This can be attributed to the influence of the inner fusion barriers. The formation of the compound nucleus requires overcoming the inner fusion barrier; otherwise, quasi-fission occurs. At higher E^*_{CN}, the impediment from the inner fusion barrier fades, leading to a higher fusion probability and diminished isotopic dependence. In Fig. 3b, the inner fusion barrier height B_{fus} of the Pu-based reactions are presented. The B_{fus} exhibits a slight variation of approximately 0.1 MeV, resulting in minimal differences in the fusion probabilities, less than an order of magnitude.

Within the framework of the dinuclear system model, the survival process is independent of the formation of the compound nucleus. The isotopic dependence of the target primarily affects the neutron richness of the formed compound nucleus. Figures 4a, b display the survival probabilities of the compound nuclei formed via the reactions ^{48}Ca + ^{239,240,242,244}Pu in the 3n- and 4n-emission channels at different E^*_{CN}. It is observed that as the E^*_{CN} increases, the survival probabilities diminish, suggesting that the compound nucleus becomes less stable and is more likely to undergo fission at high E^*_{CN}. Additionally, both Fig. 4a, b reveal an enhancement in the survival probability with the neutron-rich target. This trend is due to the enhanced stability of the formed compound nucleus as it approaches a closed neutron shell.

Notably, the variation in the survival probabilities in the 3n-emission channel is approximately an order of magnitude, whereas in the 4n-emission channel, the variation is approximately two orders of magnitude. This can be attributed to the influence of the fission barrier height B_f^M. Within the DNS model, the survival probability is determined by the competition between fission and neutron emission. In Fig. 4c, the B_f^M values are presented. This reveals that as the formed compound nucleus approaches the closed neutron shell $N = 184$, the B_f^M value increases, resulting in a suppressed possibility of fission, thereby enhancing the survival probability. The impact of the fission barrier is more pronounced in the calculation of survival probabilities in the 4n-emission channel owing to the additional competition between neutron emission and fission. Hence, with an increase in the neutron number of the target nucleus, a more significant enhancement in the survival probability was observed in the 4n-emission channel. The investigation of the capture, fusion, and

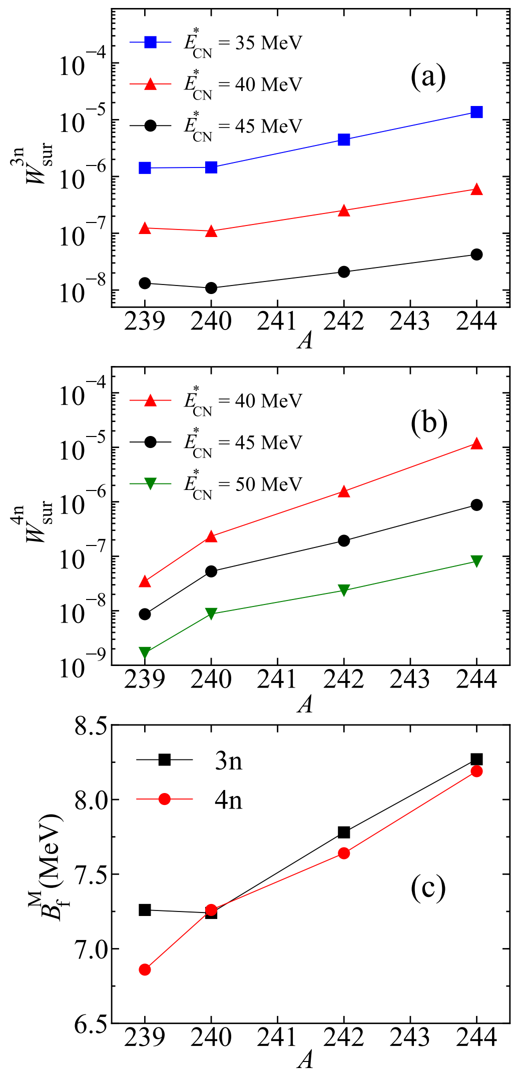

Fig. 4 (Color online) **a** The calculated survival probabilities in the 3n-emission channel for the reactions ^{48}Ca + ^{239,240,242,244}Pu→ $^{287,288,290,292-xn}$Fl + xn with E^*_{CN} = 35, 40 and 45 MeV. **b** The calculated survival probabilities in the 4n-emission channel for the same reactions with E^*_{CN} = 40, 45 and 50 MeV. **c** The B^M_f values of the corresponding emission channel for the reactions ^{48}Ca + ^{239,240,242,244}Pu→ $^{287,288,290,292-xn}$Fl + xn

survival stages reveals a substantial enhancement in the survival probabilities of the compound nuclei formed by the neutron-rich Pu targets. This enhancement significantly contributes to the observed high ER cross section.

3.2 The synthesis of new superheavy nuclei with $^{242-248}$Cm targets

In Fig. 5, the comparative analysis between calculated and experimental results is extended to the reactions ^{48}Ca + ^{245}Cm→$^{293-xn}$Lv + xn and ^{48}Ca + ^{248}Cm→$^{296-xn}$Lv + xn. The theoretical results for both reactions are in agreement with the experimental results in the 3n-emission channel. For the 4n-emission channel, the calculated ER cross sections were consistent with the experimental results for the reaction ^{48}Ca + ^{245}Cm, while the calculated maximal ER cross section for the reaction ^{48}Ca + ^{248}Cm exceeded the currently available experimental results. Investigations into the Pu- and Cm-based reactions prove not only the reliability of the DNS model but also its potential in identifying the optimal projectile–target combinations for the synthesis of new superheavy nuclei with Cm targets.

In Table 1, the optimal reaction systems, alongside the corresponding $E_{c.m.}$, E^*_{CN} and the maximal ER cross sections of the reaction systems with ^{45}Sc, ^{50}Ti, ^{51}V, ^{54}Cr, ^{55}Mn projectiles and $^{242-248}$Cm targets are presented. This indicates an exponential decrease in the maximal ER cross sections with an increase in the charge number of the formed compound nuclei. The comprehensive analysis in Table 1 reveals a dominance of the 3n-emission channel in the synthesis of new superheavy nuclei via the Cm-based reactions. An exception is observed in the synthesis of the isotope ^{293}Og, where the reaction ^{50}Ti + ^{247}Cm → ^{293}Og+4n exhibits a calculated maximal ER cross section of 114 fb. This value slightly exceeds the maximal ER cross section of 102 fb for the reaction ^{50}Ti + ^{246}Cm → ^{293}Og+3n. For the synthesis of SHE with $Z = 119$, the maximal ER cross section of 144 fb appears in the reaction ^{51}V + ^{245}Cm → ^{293}119+3n. However, the synthesis of SHEs with $Z = 120$

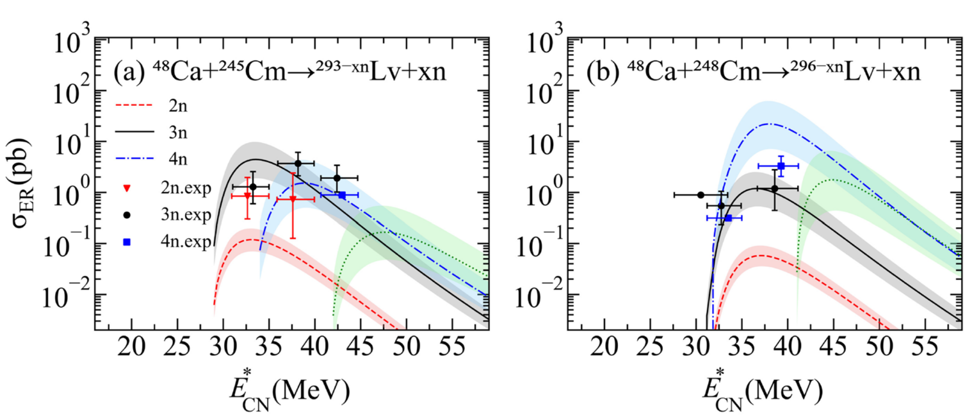

Fig. 5 (Color online) Comparison of the calculated results with the available experimental data of the reactions ^{48}Ca + ^{245,248}Cm→ $^{293,296-xn}$Lv + xn [6, 34, 35]

Table 1 The optimal Cm-based reaction systems for producing new superheavy nuclei with $Z = 117$–121

Isotope	Reaction	$E_{c.m.}$ (MeV)	E^*_{CN} (MeV)	σ^{max}_{ER} (fb)
^{284}Ts	^{242}Cm (^{45}Sc, 3n)	209.0	38.0	52^{+45}_{-25}
^{285}Ts	^{243}Cm (^{45}Sc, 3n)	205.7	36.0	497^{+465}_{-250}
^{286}Ts	^{244}Cm (^{45}Sc, 3n)	204.6	36.0	200^{+197}_{-103}
^{287}Ts	^{245}Cm (^{45}Sc, 3n)	202.2	35.0	1505^{+1554}_{-797}
^{288}Ts	^{246}Cm (^{45}Sc, 3n)	202.0	36.0	457^{+479}_{-243}
^{289}Ts	^{247}Cm (^{45}Sc, 3n)	199.7	35.0	2430^{+2641}_{-1318}
^{290}Ts	^{248}Cm (^{45}Sc, 3n)	200.3	37.0	468^{+508}_{-253}
^{289}Og	^{242}Cm (^{50}Ti, 3n)	226.1	36.0	37^{+38}_{-20}
^{290}Og	^{243}Cm (^{50}Ti, 3n)	224.3	35.0	123^{+130}_{-66}
^{291}Og	^{244}Cm (^{50}Ti, 3n)	223.5	35.0	110^{+120}_{-60}
^{292}Og	^{245}Cm (^{50}Ti, 3n)	221.4	34.0	302^{+344}_{-167}
^{293}Og	^{247}Cm (^{50}Ti, 4n)	224.8	39.0	114^{+202}_{-75}
^{295}Og	^{248}Cm (^{50}Ti, 3n)	220.0	35.0	170^{+191}_{-93}
^{290}119	^{242}Cm (^{51}V, 3n)	237.0	36.0	8^{+8}_{-4}
^{291}119	^{243}Cm (^{51}V, 3n)	234.9	35.0	56^{+58}_{-30}
^{292}119	^{244}Cm (^{51}V, 3n)	233.9	35.0	26^{+27}_{-14}
^{293}119	^{245}Cm (^{51}V, 3n)	230.8	33.0	144^{+157}_{-79}
^{294}119	^{246}Cm (^{51}V, 3n)	231.7	35.0	21^{+23}_{-11}
^{295}119	^{247}Cm (^{51}V, 3n)	228.8	33.0	73^{+80}_{-40}
^{296}119	^{248}Cm (^{51}V, 3n)	230.0	35.0	10^{+10}_{-5}
^{293}120	^{242}Cm (^{54}Cr, 3n)	248.6	37.0	$0.278^{+0.259}_{-0.139}$
^{294}120	^{243}Cm (^{54}Cr, 3n)	246.9	36.0	$0.699^{+0.658}_{-0.353}$
^{295}120	^{244}Cm (^{54}Cr, 3n)	246.7	37.0	$0.177^{+0.166}_{-0.089}$
^{296}120	^{245}Cm (^{54}Cr, 3n)	245.0	36.0	$0.387^{+0.364}_{-0.195}$
^{297}120	^{246}Cm (^{54}Cr, 3n)	244.1	36.0	$0.231^{+0.220}_{-0.117}$
^{298}120	^{247}Cm (^{54}Cr, 3n)	242.3	35.0	$0.877^{+0.821}_{-0.443}$
^{299}120	^{248}Cm (^{54}Cr, 3n)	242.1	34.0	$0.247^{+0.220}_{-0.120}$
^{294}121	^{242}Cm (^{55}Mn, 3n)	259.1	38.0	$0.007^{+0.005}_{-0.003}$
^{295}121	^{243}Cm (^{55}Mn, 3n)	256.9	37.0	$0.027^{+0.022}_{-0.012}$
^{296}121	^{244}Cm (^{55}Mn, 3n)	255.8	37.0	$0.011^{+0.009}_{-0.005}$
^{297}121	^{245}Cm (^{55}Mn, 3n)	253.6	36.0	$0.029^{+0.024}_{-0.014}$
^{298}121	^{246}Cm (^{55}Mn, 3n)	253.7	37.0	$0.012^{+0.010}_{-0.006}$
^{299}121	^{247}Cm (^{55}Mn, 3n)	251.5	36.0	$0.052^{+0.044}_{-0.025}$
^{300}121	^{248}Cm (^{55}Mn, 3n)	250.7	36.0	$0.031^{+0.025}_{-0.014}$

The isotopes, reaction systems, optimal incident energy $E_{c.m.}$, E^*_{CN} and maximal calculated ER cross sections are listed in columns 1–5, respectively. Theoretical computational uncertainties arise from the E_D range

and 121 exhibits significantly reduced maximal ER cross sections of 0.877 fb for the reaction ^{54}Cr + ^{247}Cm → ^{298}120+3n and 0.052 fb for the reaction ^{55}Mn + ^{247}Cm → ^{299}121+3n, respectively, which can be attributed to the increase in the mass number of the projectile.

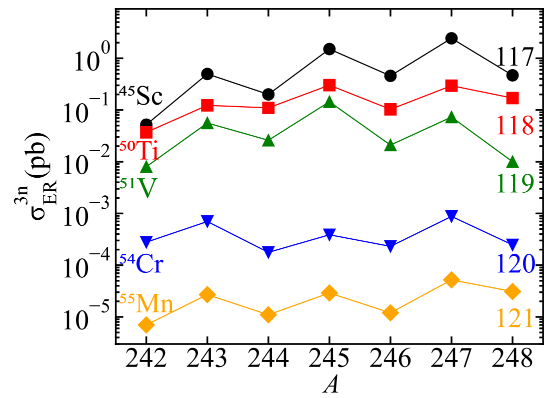

Fig. 6 (Color online) The calculated maximal ER cross sections in the 3n-emission channel for synthesizing new superheavy nuclei with $Z = 117$–121 via the combinations of the ^{45}Sc, ^{50}Ti, ^{51}V, ^{54}Cr and ^{55}Mn projectiles and the $^{242-248}$Cm targets

3.3 The isotopic dependence of the reactions with $^{242-248}$Cm targets

To further investigate the isotopic dependence of the $^{242-248}$Cm target, the calculated maximal ER cross sections of the Cm-based reactions in the 3n-emission channel are plotted in Fig. 6. An increasing trend in the maximal ER cross sections was observed as the neutron excess in the Cm target increased. This trend is accompanied by an apparent odd–even staggering, indicating the advantage of neutron-rich Cm targets with odd neutron numbers. To further discuss this phenomenon, the capture, fusion, and survival stages are discussed in Fig. 7.

In Fig. 7a, the capture cross sections of the reaction systems with ^{45}Sc, ^{50}Ti, ^{51}V, ^{54}Cr, ^{55}Mn projectiles and $^{242-248}$Cm targets are presented. Consistent with the aforementioned discussion, the capture cross sections displayed a decreasing trend as the neutron number of the target increased. For ^{45}Sc-induced reactions, the isotopic effect on the capture was relatively significant. For the other reactions, the capture cross section exhibited considerably less variation. Figure 7b presents the fusion probabilities of the corresponding reactions. A significant decline in the fusion probabilities was observed between the ^{45}Sc- and ^{50}Ti-induced reactions, as well as the ^{51}V- and ^{54}Cr-induced reactions. This can be ascribed to the varying mass asymmetry values influenced by the projectile mass numbers. In Fig. 7b, a decreasing trend in the fusion probabilities with an increasing neutron number of the target can be observed. This isotopic-dependent decreasing trend in the fusion probability, along with the same trend discussed in Fig. 3, can be attributed to the deviation in the neutron number of the target from the closed neutron shell [89]. Furthermore, an odd–even effect can also be noted, which can be attributed to the pairing effect in the fusion stage.

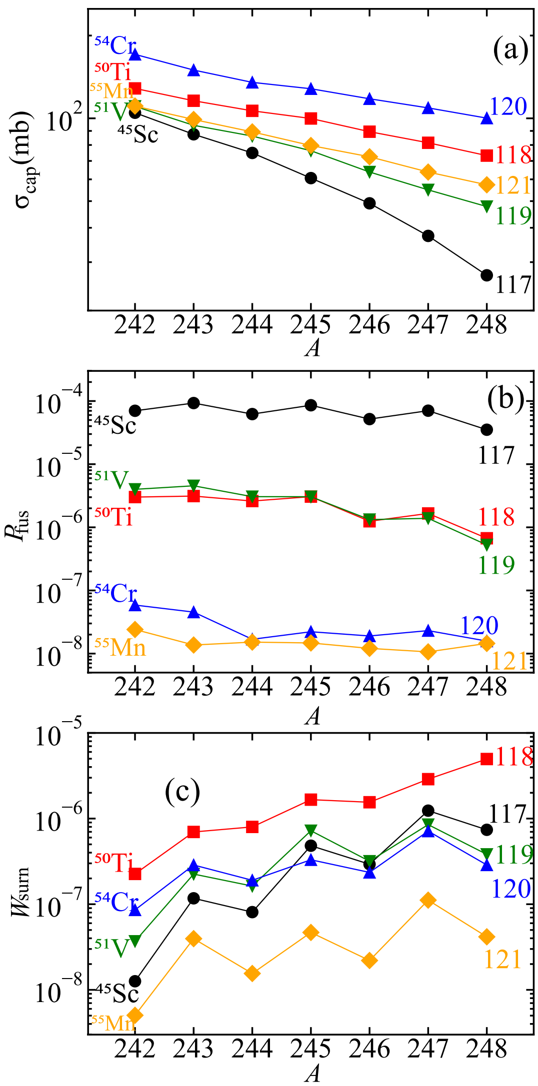

Fig. 7 (Color online) **a** The capture cross sections, **b** the fusion probabilities, and **c** the survival probabilities at $E^*_{CN} = 35$ MeV for synthesizing new superheavy nuclei with $Z = 117$–121 via the combinations of the ^{45}Sc, ^{50}Ti, ^{51}V, ^{54}Cr and ^{55}Mn projectiles and the $^{242-248}$Cm targets

In Fig. 7c, the survival probabilities of the corresponding reactions in the 3n-emission channel are presented. As the neutron number of the formed compound nucleus approaches the predicted closed neutron shell $N = 184$, the stability of the compound nucleus is enhanced, leading to ascending survival probabilities with increasing neutron excess in the target. The odd–even effect is also significant, which primarily arises from the influence of the variance of the fission barrier. For reactions synthesizing superheavy nuclei with $Z = 117$, the survival probability increases rapidly as the neutron number of the target increases. This trend can be attributed to the neutron number of the formed compound nuclei approaching the semi-closed neutron shell at $N = 178$. It was also observed that for reactions involving even–even projectiles such as ^{50}Ti and ^{54}Cr, the odd–even effect was suppressed. This reduction in the odd–even effect can be ascribed to the pairing effects. It is evident that, in the synthesis of new superheavy nucleus via the $^{242-248}$Cm targets, the isotopic dependence on the maximal ER cross section mainly arises from the survival stages. Here, the odd–even effect, coupled with the high neutron excess of the target, strongly enhances the stability of the formed compound nucleus. Consequently, the ^{247}Cm target is favorable for the future synthesis of superheavy nuclei.

4 Summary

In this study, the predictive reliability of the DNS model on isotopic dependence was examined using experimental results for the reactions ^{48}Ca + ^{239,240,242,244}Pu. The impact of the target isotope is discussed in the capture, fusion, and survival stages, revealing a strong enhancement in the survival probabilities owing to the influence of the fission barrier height. The feasibility of applying the $^{242-248}$Cm targets and the stable projectiles ^{45}Sc, ^{50}Ti, ^{51}V, ^{54}Cr, ^{55}Mn for synthesizing new superheavy nuclei $^{284-290}$Ts, $^{289-293,295}$Og, $^{290-296}$119, $^{293-299}$120, $^{294-300}$121 is investigated. To synthesize new superheavy elements with $Z = 119$–121, the optimal reaction systems are predicted to be the reactions ^{51}V + ^{245}Cm → ^{293}119 + 3n, ^{54}Cr + ^{247}Cm → ^{298}120 + 3n, and ^{55}Mn + ^{247}Cm → ^{299}121 + 3n, with the maximal ER cross sections of 144 fb, 0.877 fb, and 0.052 fb, respectively. The isotopic dependence of the maximal ER cross sections of the $^{242-248}$Cm-based reactions was investigated in detail, indicating that the isotopic dependence of the Cm targets mainly arises from the survival stages. This is attributed to the enhanced stability of the formed compound nuclei, influenced by a higher neutron number when approaching the predicted neutron shell closure $N = 184$. The odd–even effect coupled with the high neutron excess renders the ^{247}Cm target promising for the future synthesis of superheavy nuclei.

Author Contributions All authors contributed to the conception and design of the study. Material preparation, data collection and analysis were performed by Ming-Hao Zhang, Mei-Chen Wang, Ying Zou, Gen Zhang, Qing-Lin Niu, and Feng-Shou Zhang. The first draft of the manuscript was written by Ming-Hao Zhang, and all authors commented on previous versions of the manuscript. All authors read and approved the final manuscript.

Data availability The data that support the findings of this study are openly available in Science Data Bank at https://cstr.cn/31253.11.sciencedb.j00186.00966 and https://doi.org/10.57760/sciencedb.j00186.00966.

Declarations

Conflict of interest Feng-Shou Zhang is an editorial board member for Nuclear Science and Techniques and was not involved in the editorial review, or the decision to publish this article. All authors declare that there are no Conflict of interest.

References

1. P. Möller, A. Sierk, T. Ichikawa et al., Nuclear ground-state masses and deformations: FRDM(2012). At. Data Nucl. Data Tables **109–110**, 1–204 (2016). https://doi.org/10.1016/j.adt.2015.10.002
2. S. Ćwiok, P.H. Heenen, W. Nazarewicz, Shape coexistence and triaxiality in the superheavy nuclei. Nature **433**, 705–709 (2005). https://doi.org/10.1038/nature03336
3. A.T. Kruppa, M. Bender, W. Nazarewicz et al., Shell corrections of superheavy nuclei in self-consistent calculations. Phys. Rev. C **61**, 034313 (2000). https://doi.org/10.1103/PhysRevC.61.034313
4. D. Ackermann, C. Theisen, Nuclear structure features of very heavy and superheavy nuclei-tracing quantum mechanics towards the "island of stability''. Phys. Scr. **92**(8), 083002 (2017). https://doi.org/10.1088/1402-4896/aa7921
5. M.H. Zhang, Y. Zou, M.C. Wang et al., Possibility of reaching the predicted center of the "island of stability'' via the radioactive beam-induced fusion reactions. Nucl. Sci. Tech. **35**, 161 (2024). https://doi.org/10.1007/s41365-024-01542-x
6. Y.T. Oganessian, V.K. Utyonkov, Y.V. Lobanov et al., Synthesis of the isotopes of elements 118 and 116 in the ^{249}Cf and ^{245}Cm $+^{48}$ Ca fusion reactions. Phys. Rev. C **74**, 044602 (2006). https://doi.org/10.1103/PhysRevC.74.044602
7. Y.T. Oganessian, A. Yeremin, A. Popeko et al., Synthesis of nuclei of the superheavy element 114 in reactions induced by ^{48} Ca. Nature **400**, 242 (1999). https://doi.org/10.1038/22281
8. Y.T. Oganessian, F.S. Abdullin, S.N. Dmitriev et al., Investigation of the ^{243}Am+ ^{48} Ca reaction products previously observed in the experiments on elements 113, 115, and 117. Phys. Rev. C **87**, 014302 (2013). https://doi.org/10.1103/PhysRevC.87.014302
9. Y.T. Oganessian, V.K. Utyonkov, Y.V. Lobanov et al., Observation of the decay of ^{292}116. Phys. Rev. C **63**, 011301(R) (2000). https://doi.org/10.1103/PhysRevC.63.011301
10. Y.T. Oganessian, F.S. Abdullin, P.D. Bailey et al., Synthesis of a new element with atomic number $Z = 117$. Phys. Rev. Lett. **104**, 142502 (2010). https://doi.org/10.1103/PhysRevLett.104.142502
11. M.H. Zhang, Y.H. Zhang, J.J. Li et al., Progress in transport models of heavy-ion collisions for the synthesis of superheavy nuclei. Nuclear Techniques (in Chinese) **46**, 080014 (2023). https://doi.org/10.11889/j.0253-3219.2023.hjs.46.080014
12. T. Huang, D. Seweryniak, B.B. Back et al., Discovery of the new isotope ^{251}Lr: impact of the hexacontetrapole deformation on single-proton orbital energies near the $Z = 100$ deformed shell gap. Phys. Rev. C **106**, L061301 (2022). https://doi.org/10.1103/PhysRevC.106.L061301
13. K. Morita, K. Morimoto, D. Kaji et al., Experiment on the synthesis of element 113 in the reaction ^{209}Bi (^{70}Zn, n) ^{278}113. J. Phys. Soc. Jpn. **73**, 2593 (2004). https://doi.org/10.1143/jpsj.73.2593
14. Y.T. Oganessian, V.K. Utyonkov, Super-heavy element research. Rep. Prog. Phys. **78**(3), 036301 (2015). https://doi.org/10.1088/0034-4885/78/3/036301
15. Y. Oganessian, V. Utyonkov, Superheavy nuclei from ^{48}Ca-induced reactions. Nucl. Phys. A **944**, 62–98 (2015). https://doi.org/10.1016/j.nuclphysa.2015.07.003
16. M. Thoennessen, Discovery of isotopes of elements with $Z \geq 100$. At. Data Nucl. Data Tables **99**(3), 312–344 (2013). https://doi.org/10.1016/j.adt.2012.03.003
17. Z.Y. Zhang, Z.G. Gan, L. Ma et al., Observation of the superheavy nuclide ^{271}Ds. Chin. Phys. Lett. **29**(1), 012502 (2012). https://doi.org/10.1088/0256-307X/29/1/012502
18. Y.T. Oganessian, V.K. Utyonkov, N.D. Kovrizhnykh et al., New isotope ^{286}Mc produced in the ^{243}Am+^{48}Ca reaction. Phys. Rev. C **106**, 064306 (2022). https://doi.org/10.1103/PhysRevC.106.064306
19. S. Hofmann, Synthesis of superheavy elements by cold fusion. Radiochim. Acta **99**, 405–428 (2011). https://doi.org/10.1524/ract.2011.1854
20. M.H. Zhang, Z.Y. Zhang, Z.G. Gan et al., Progress on the synthesis of superheavy nuclei. Nucl. Sci. Tech. **36**, 204 (2025). https://doi.org/10.1007/s41365-025-01781-6
21. S.M. Robinson, J. Allender, N. Bridges et al., Recovery of mark-18a (mk-18a) target materials: program management plan. Tech. rep., Oak Ridge National Lab. (ORNL), Oak Ridge (2014). https://doi.org/10.2172/1159480
22. V.K. Utyonkov, N.T. Brewer, Y.T. Oganessian et al., Experiments on the synthesis of superheavy nuclei ^{284}Fl and ^{285}Fl in the ^{239,240}Pu $+^{48}$ Ca reactions. Phys. Rev. C **92**, 034609 (2015). https://doi.org/10.1103/PhysRevC.92.034609
23. V.K. Utyonkov, N.T. Brewer, Y.T. Oganessian et al., Neutron-deficient superheavy nuclei obtained in the ^{240}Pu $+^{48}$ Ca reaction. Phys. Rev. C **97**, 014320 (2018). https://doi.org/10.1103/PhysRevC.97.014320
24. Y.T. Oganessian, V.K. Utyonkov, D. Ibadullayev et al., Investigation of ^{48}Ca-induced reactions with ^{242}Pu and ^{238}U targets at the jinr superheavy element factory. Phys. Rev. C **106**, 024612 (2022). https://doi.org/10.1103/PhysRevC.106.024612
25. L. Stavsetra, K.E. Gregorich, J. Dvorak et al., Independent verification of element 114 production in the ^{48}Ca $+^{242}$ Pu reaction. Phys. Rev. Lett. **103**, 132502 (2009). https://doi.org/10.1103/PhysRevLett.103.132502
26. P.A. Ellison, K.E. Gregorich, J.S. Berryman et al., New superheavy element isotopes: ^{242}Pu(^{48}Ca, 5n)^{285}114. Phys. Rev. Lett. **105**, 182701 (2010). https://doi.org/10.1103/PhysRevLett.105.182701
27. J.M. Gates, C.E. Düllmann, M. Schädel et al., First superheavy element experiments at the GSI recoil separator TASCA: The production and decay of element 114 in the ^{244}Pu(^{48}Ca,3–4n) reaction. Phys. Rev. C **83**, 054618 (2011). https://doi.org/10.1103/PhysRevC.83.054618
28. T. Sikkeland, A. Ghiorso, M.J. Nurmia, Analysis of excitation functions in Cm(C, xn)No reactions. Phys. Rev. **172**, 1232–1238 (1968). https://doi.org/10.1103/PhysRev.172.1232
29. M. Murakami, S. Goto, H. Murayama et al., Excitation functions for production of rf isotopes in the ^{248}Cm $+^{18}$O reaction. Phys. Rev. C **88**, 024618 (2013). https://doi.org/10.1103/PhysRevC.88.024618
30. Y. Nagame, M. Asai, H. Haba et al., Status and prospects of heavy element nuclear chemistry research at Jaeri. J. Nucl. Radiochem. Sci. **3**(1), 129 (2002). https://doi.org/10.14494/jnrs2000.3.129
31. H. Haba, M. Huang, D. Kaji et al., Production of ^{262}Db in the ^{248}Cm(^{19}F,5n)^{262}Db reaction and decay properties of ^{262}Db and ^{258}Lr. Phys. Rev. C **89**, 024618 (2014). https://doi.org/10.1103/PhysRevC.89.024618
32. H. Haba, D. Kaji, Y. Kudou et al., Production of ^{265}Sg in the ^{248} Cm(^{22}Ne,5n)^{265}Sg reaction and decay properties of two isomeric states in ^{265}Sg. Phys. Rev. C **85**, 024611 (2012). https://doi.org/10.1103/PhysRevC.85.024611
33. J. Dvorak, W. Brüchle, M. Chelnokov et al., Observation of the 3n evaporation channel in the complete hot-fusion reaction

^{26}Mg +^{248} Cm leading to the new superheavy nuclide ^{271}Hs. Phys. Rev. Lett. **100**, 132503 (2008). https://doi.org/10.1103/PhysRevLett.100.132503
34. Y.T. Oganessian, V.K. Utyonkov, Y.V. Lobanov et al., Measurements of cross sections for the fusion-evaporation reactions ^{244} Pu (^{48} Ca, xn) $^{292-x}$ 114 and ^{245} Cm (^{48} Ca, xn) $^{293-x}$ 116. Phys. Rev. C **69**(5), 054607 (2004). https://doi.org/10.1103/PhysRevC.69.054607
35. Y.T. Oganessian, V.K. Utyonkov, Y.V. Lobanov et al., Measurements of cross sections and decay properties of the isotopes of elements 112, 114, and 116 produced in the fusion reactions ^{233,238}U, ^{242}Pu, and ^{248}Cm + ^{48}Ca. Phy. Rev. C **70**(6), 064609 (2004). https://doi.org/10.1103/PhysRevC.70.064609
36. F.P. Heßberger, D. Ackermann, Some critical remarks on a sequence of events interpreted to possibly originate from a decay chain of an element 120 isotope. Eur. Phys. J. A **53**(6), 1–9 (2017). https://doi.org/10.1140/epja/i2017-12307-5
37. D. Hartanto, D. Chandler, J.W. Bae et al., ^{252}cf production at the high flux isotope reactor: nuclear data selection and leu conversion impacts, Tech. rep., Oak Ridge National Laboratory (ORNL), Oak Ridge (2023)
38. M. Tanaka, P. Brionnet, M. Du et al., Probing optimal reaction energy for synthesis of element 119 from ^{51}V+^{248}Cm reaction with quasielastic barrier distribution measurement. J. Phys. Soc. Jpn. **91**(8), 084201 (2022). https://doi.org/10.7566/JPSJ.91.084201
39. K. Siwek-Wilczyńska, T. Cap, M. Kowal et al., Predictions of the fusion-by-diffusion model for the synthesis cross sections of Z = 114–120 elements based on macroscopic-microscopic fission barriers. Phys. Rev. C **86**, 014611 (2012). https://doi.org/10.1103/PhysRevC.86.014611
40. L. Liu, C.W. Shen, Q.F. Li et al., Residue cross sections of ^{50}Ti-induced fusion reactions based on the two-step model. Eur. Phys. J. A **52**, 35–39 (2016). https://doi.org/10.1140/epja/i2016-16035-0
41. C.W. Shen, Y. Abe, D. Boilley et al., Isospin dependence of reactions ^{48}Ca+$^{243-251}$Bk. Int. J. Mod. Phys. E **17**, 66–79 (2008). https://doi.org/10.1142/S0218301308011768
42. D. Boilley, Y. Abe, B. Cauchois et al., Elimination of fast variables and initial slip: a new mechanism for fusion hindrance in heavy-ion collisions. J. Phys. G Nucl. Part. Phys. **46**(11), 115102 (2019). https://doi.org/10.1088/1361-6471/ab11ef
43. V. Zagrebaev, W. Greiner, Cross sections for the production of superheavy nuclei. Nucl. Phys. A **944**, 257–307 (2015). https://doi.org/10.1016/j.nuclphysa.2015.02.010
44. S. Amano, Y. Aritomo, M. Ohta, Dynamical mechanism of fusion hindrance in heavy ion collisions. Phys. Rev. C **108**, 014612 (2023). https://doi.org/10.1103/PhysRevC.108.014612
45. N. Wang, Z. Li, X. Wu, Improved quantum molecular dynamics model and its applications to fusion reaction near barrier. Phys. Rev. C **65**, 064608 (2002). https://doi.org/10.1103/PhysRevC.65.064608
46. X.X. Sun, L. Guo, Microscopic study of the hot-fusion reaction ^{48}Ca +^{238} U with the constraints from time-dependent Hartree-Fock theory. Phys. Rev. C **107**, 064609 (2023). https://doi.org/10.1103/PhysRevC.107.064609
47. R. Gumbel, C. Ross, A.S. Umar, Role of isospin composition in low-energy nuclear fusion. Phys. Rev. C **108**, L051602 (2023). https://doi.org/10.1103/PhysRevC.108.L051602
48. A.S. Umar, V.E. Oberacker, J.A. Maruhn et al., Entrance channel dynamics of hot and cold fusion reactions leading to superheavy elements. Phys. Rev. C **81**, 064607 (2010). https://doi.org/10.1103/PhysRevC.81.064607
49. K. Sekizawa, K. Hagino, Time-dependent Hartree–Fock plus Langevin approach for hot fusion reactions to synthesize the Z = 120 superheavy element. Phys. Rev. C **99**, 051602(R) (2019). https://doi.org/10.1103/PhysRevC.99.051602
50. L.L. Zhou, J.J. Cai, L.Q. Li et al., Fusion enhancement in the collisions with ^{44}Ca beams and the production of neutron-deficient $^{245-250}$Lr isotopes. Phys. Rev. C **109**, 024606 (2024). https://doi.org/10.1103/PhysRevC.109.024606
51. L. Guo, C.W. Shen, C. Yu et al., Isotopic trends of quasifission and fusion-fission in the reactions ^{48}Ca +^{239,244} Pu. Phys. Rev. C **98**, 064609 (2018). https://doi.org/10.1103/PhysRevC.98.064609
52. N. Wang, E.G. Zhao, W. Scheid et al., Theoretical study of the synthesis of superheavy nuclei with Z = 119 and 120 in heavy-ion reactions with trans-uranium targets. Phys. Rev. C **85**, 041601 (2012). https://doi.org/10.1103/PhysRevC.85.041601
53. X.J. Bao, Possibility to produce ^{293,295,296}Og in the reactions ^{48}Ca +^{249,250,251} Cf. Phys. Rev. C **100**, 011601 (2019). https://doi.org/10.1103/PhysRevC.100.011601
54. L. Zhu, Law of optimal incident energy for synthesizing superheavy elements in hot fusion reactions. Phys. Rev. Res. **5**, L022030 (2023). https://doi.org/10.1103/PhysRevResearch.5.L022030
55. L. Zhu, J. Su, F.S. Zhang, Influence of the neutron numbers of projectile and target on the evaporation residue cross sections in hot fusion reactions. Phys. Rev. C **93**, 064610 (2016). https://doi.org/10.1103/PhysRevC.93.064610
56. J.J. Li, N. Tang, Y.H. Zhang et al., Progress on production cross-sections of unknown nuclei in fusion evaporation reactions and multinucleon transfer reactions. Int. J. Mod. Phys. E **32**(01), 2330002 (2023). https://doi.org/10.1142/S0218301323300023
57. A. Nasirov, B. Kayumov, Optimal colliding energy for the synthesis of a superheavy element with Z = 119. Phys. Rev. C **109**, 024613 (2024). https://doi.org/10.1103/PhysRevC.109.024613
58. L.Q. Li, G. Zhang, F.S. Zhang, Production of unknown Fl isotopes in proton evaporation channels within the Dinuclear system model. Phys. Rev. C **106**, 024601 (2022). https://doi.org/10.1103/PhysRevC.106.024601
59. L. Zhu, W.J. Xie, F.S. Zhang, Production cross sections of superheavy elements Z = 119 and 120 in hot fusion reactions. Phys. Rev. C **89**, 024615 (2014). https://doi.org/10.1103/PhysRevC.89.024615
60. X.J. Bao, Y. Gao, J.Q. Li et al., Isotopic dependence of superheavy nuclear production in hot fusion reactions. Phys. Rev. C **92**, 034612 (2015). https://doi.org/10.1103/PhysRevC.92.034612
61. G.G. Adamian, N.V. Antonenko, W. Scheid, Isotopic trends in the production of superheavy nuclei in cold fusion reactions. Phys. Rev. C **69**, 011601 (2004). https://doi.org/10.1103/PhysRevC.69.011601
62. M.H. Zhang, Y. Zou, M.C. Wang et al., Predictions for the synthesis of new superheavy nuclei with a ^{252}Cf target. Chin. Phys. C **49**, 054107 (2025). https://doi.org/10.1088/1674-1137/ada3cc
63. J. Khuyagbaatar, A. Yakushev, C.E. Düllmann et al., Search for elements 119 and 120. Phys. Rev. C **102**, 064602 (2020). https://doi.org/10.1103/PhysRevC.102.064602
64. A.K. Nasirov, A.R. Yusupov, B.M. Kayumov, Small cross section of the synthesis of darmstadtium in the ^{48}Ca +^{232} Th reaction. Phys. Rev. C **110**(1), 014618 (2024). https://doi.org/10.1103/PhysRevC.110.014618
65. V.I. Zagrebaev, Synthesis of superheavy nuclei: nucleon collectivization as a mechanism for compound nucleus formation. Phys. Rev. C **64**, 034606 (2001). https://doi.org/10.1103/PhysRevC.64.034606
66. A.S. Zubov, G.G. Adamian, N.V. Antonenko et al., Survival probability of superheavy nuclei. Phys. Rev. C **65**, 024308 (2002). https://doi.org/10.1103/PhysRevC.65.024308
67. W.D. Myers, W.J. Swiatecki, Nuclear masses and deformations. Nucl. Phys. **81**(1), 1–60 (1966). https://doi.org/10.1016/0029-5582(66)90639-0

68. M.H. Zhang, M.C. Wang, Y. Zou et al., Predictions for the synthesis of unknown $^{279-281}$Nh and ^{287,288}Nh isotopes. Phys. Rev. C **111**, 024611 (2025). https://doi.org/10.1103/PhysRevC.111.024611
69. C.Y. Wong, Interaction barrier in charged-particle nuclear reactions. Phys. Rev. Lett. **31**, 766–769 (1973). https://doi.org/10.1103/PhysRevLett.31.766
70. Q.F. Li, W. Zuo, W.F. Li et al., Deformation and orientation effects in the driving potential of the Dinuclear model. Eur. Phys. J. A—Hadrons Nucl. **24**, 223–229 (2005). https://doi.org/10.1140/epja/i2004-10138-1
71. Z. Ahmed, Tunnelling through the Morse barrier. Phys. Lett. A **157**, 1–5 (1991). https://doi.org/10.1016/0375-9601(91)90399-S
72. V.Y. Denisov, Expression for the heavy-ion fusion cross section. Phys. Rev. C **107**, 054618 (2023). https://doi.org/10.1103/PhysRevC.107.054618
73. M.H. Zhang, Y.H. Zhang, Y. Zou et al., Predictions of synthesizing elements with $Z = 119$ and 120 in fusion reactions. Phys. Rev. C **109**, 014622 (2024). https://doi.org/10.1103/PhysRevC.109.014622
74. B. Wang, K. Wen, W.J. Zhao et al., Systematics of capture and fusion dynamics in heavy-ion collisions. At. Data Nucl. Data Tables **114**, 281–370 (2017). https://doi.org/10.1016/j.adt.2016.06.003
75. V.Y. Denisov, Compound nucleus formation cross sections in lead-induced reactions. Phys. Rev. C **111**(2), 024601 (2025). https://doi.org/10.1103/PhysRevC.111.024601
76. G.G. Adamian, N.V. Antonenko, R.V. Jolos, Mass parameters for a Dinuclear system. Nucl. Phys. A **584**(1), 205–220 (1995). https://doi.org/10.1016/0375-9474(94)00505-H
77. B.M. Kayumov, O.K. Ganiev, A.K. Nasirov et al., Analysis of the fusion mechanism in the synthesis of superheavy element 119 via the ^{54}Cr $+^{243}$ Am reaction. Phys. Rev. C **105**(1), 014618 (2022). https://doi.org/10.1103/PhysRevC.105.014618
78. J.Q. Li, G. Wolschin, Distribution of the dissipated angular momentum in heavy-ion collisions. Phys. Rev. C **27**, 590–601 (1983). https://doi.org/10.1103/PhysRevC.27.590
79. S. Ayik, B. Schürmann, W. Nörenberg, Microscopic transport theory of heavy-ion collisions. Z. Phys. A **277**(3), 299–310 (1976). https://doi.org/10.1007/BF01415605
80. G.G. Adamian, N.V. Antonenko, W. Scheid, Characteristics of quasifission products within the Dinuclear system model. Phys. Rev. C **68**, 034601 (2003). https://doi.org/10.1103/PhysRevC.68.034601
81. J.D. Jackson, A schematic model for (p, xn) cross sections in heavy elements. Can. J. Phys. **34**, 767–779 (1956). https://doi.org/10.1139/p56-087
82. V. Weisskopf, Statistics and nuclear reactions. Phys. Rev. **52**, 295–303 (1937). https://doi.org/10.1103/PhysRev.52.295
83. N. Bohr, J.A. Wheeler, The mechanism of nuclear fission. Phys. Rev. **56**, 426–450 (1939). https://doi.org/10.1103/PhysRev.56.426
84. L. Zhu, Selection of projectiles for producing trans-uranium nuclei in transfer reactions within the improved Dinuclear system model. J. Phys. G Nucl. Part. Phys. **47**, 065107 (2020). https://doi.org/10.1088/1361-6471/ab871f
85. W.F. Li, Z.Z. Wang, H.S. Xu et al., Odd-Even effects of the survival probability for superheavy compound nuclei. Chin. Phys. Lett. **21**, 636 (2004). https://doi.org/10.1088/0256-307X/21/4/013
86. C.J. Xia, B.X. Sun, E.G. Zhao et al., Systematic study of survival probability of excited superheavy nuclei. Sci. China Phys. Mech. Astron. **54**, 109–113 (2011). https://doi.org/10.1007/s11433-011-4438-2
87. H. Lü, D. Boilley, Y. Abe et al., Synthesis of superheavy elements: uncertainty analysis to improve the predictive power of reaction models. Phys. Rev. C **94**, 034616 (2016). https://doi.org/10.1103/PhysRevC.94.034616
88. J.A. Sheikh, W. Nazarewicz, J.C. Pei, Systematic study of fission barriers of excited superheavy nuclei. Phys. Rev. C **80**, 011302(R) (2009). https://doi.org/10.1103/PhysRevC.80.011302
89. K.H. Schmidt, W. Morawek, The conditions for the synthesis of heavy nuclei. Rep. Prog. Phys. **54**(7), 949 (1991). https://doi.org/10.1088/0034-4885/54/7/002